REVIEW ARTICLE

New techniques for assessing response after hypofractionated radiotherapy for lung cancer

Sarah A. Mattonen[1], Kitty Huang[2,3], Aaron D. Ward[1,2], Suresh Senan[4], David A. Palma[2,3]

[1]Department of Medical Biophysics, [2]Department of Oncology, The University of Western Ontario, London, ON, Canada; [3]Division of Radiation Oncology, London Regional Cancer Program, London, ON, Canada; [4]Department of Radiation Oncology, VU University Medical Center, Amsterdam, Netherlands

ABSTRACT Hypofractionated radiotherapy (HFRT) is an effective and increasingly-used treatment for early stage non-small cell lung cancer (NSCLC). Stereotactic ablative radiotherapy (SABR) is a form of HFRT and delivers biologically effective doses (BEDs) in excess of 100 Gy_{10} in 3-8 fractions. Excellent long-term outcomes have been reported; however, response assessment following SABR is complicated as radiation induced lung injury can appear similar to a recurring tumor on CT. Current approaches to scoring treatment responses include Response Evaluation Criteria in Solid Tumors (RECIST) and positron emission tomography (PET), both of which appear to have a limited role in detecting recurrences following SABR. Novel approaches to assess response are required, but new techniques should be easily standardized across centers, cost effective, with sensitivity and specificity that improves on current CT and PET approaches. This review examines potential novel approaches, focusing on the emerging field of quantitative image feature analysis, to distinguish recurrence from fibrosis after SABR.

KEYWORDS Lung cancer; stereotactic radiotherapy; hypofractionated radiotherapy (HFRT); image feature analysis; positron emission tomography (PET)

J Thorac Dis 2014;6(4):375-386. doi: 10.3978/j.issn.2072-1439.2013.11.09

Hypofractionated radiotherapy (HFRT) for early-stage lung cancer

HFRT is an effective and well-tolerated treatment for early stage non-small cell lung cancer (NSCLC) (1,2). Although several HFRT schemes have been used historically in the treatment of T1N0 or T2N0 NSCLC, ranging from mildly hypofractionated regimens [e.g., 55 Gy in 20 fractions (3)], to more potent stereotactic regimens (e.g., 54 Gy in 3 fractions), evidence suggests that a biologically effective dose (BED) in excess of 100 Gy_{10} is required for optimal local control (4). Such stereotactic regimens, referred to as stereotactic ablative radiotherapy (SABR) or stereotactic body radiotherapy (SBRT), have been rapidly adopted into clinical use in the last decade (5). SABR is a guideline-recommended treatment for T1/T2 N0 NSCLC when surgery, the gold standard treatment, is not an option due to patient comorbidities or refusal (6-8). SABR is arguably one of the largest medical breakthroughs in the curative treatment of early stage NSCLC in the last two decades, with improved population-based survival rates demonstrated after the implementation of SABR (9-11).

Excellent long-term outcomes support this increasing popularity of SABR as a treatment option for lung cancer. SABR outcomes appear not only superior to more fractionated HFRT regimens (12), but are comparable to standard surgical resection, as supported by retrospective, single- or multi-institution, and modeling studies, with the largest single-institution retrospective study reporting a 5-year local control rate of 89.5% (13-15). Although three randomized studies comparing surgery to SABR have failed to accrue, propensity score matched analyses are available, and have shown comparable, if not superior outcomes post-SABR (16,17). In high-risk patients with severe pulmonary

Correspondence to: Dr. David A. Palma. London Regional Cancer Program, 790 Commissioners Rd E, London, Ontario, Canada. Email: david.palma@lhsc.on.ca.

Submitted Aug 23, 2013. Accepted for publication Nov 07, 2013.
Available at www.jthoracdis.com

ISSN: 2072-1439

comorbidities, SABR offers comparable rates of local control without the attendant short-term mortality risks of surgery (18). In the operable patient population, promising outcomes are reported by two prospective clinical trials: RTOG 0618, reporting a primary tumor failure rate of 7.7% (19), and JCOG 0403, reporting a preliminary 3-year tumor control rate of 86% (20). For institutions without the capability to deliver SABR, other HFRT regimens can also achieve reasonable local control at early time-points: a recent Canadian multicenter study of HFRT delivering 60 Gy in 15 fractions (BED of 75 Gy_{10}) achieved a two-year local control rate of 88% (21).

Response assessment: lung injury after SABR

Response assessment following SABR is complicated by the frequent presence of benign lung injury on follow-up CT. Ablative doses of radiation delivered to the tumor and surrounding lung parenchyma nearly always result in radiologic lung injury (pneumonitis and fibrosis), appearing as an increased density and opacity on CT in the area of the high-dose region, and occasionally a corresponding increase in metabolic activity on functional imaging in the months following SABR (22,23). Such CT changes correlate closely with local delivered dose (24). Such findings are not unique to lung SABR; they have also been described in other organs treated with stereotactic radiotherapy including brain and liver (25,26). From histopathological studies obtained after resection for false-positive imaging studies, these areas of lung injury are made up of a benign mixture of inflammatory cells, fibrocytes and other benign features (27). The appearance of fibrosis is very common, occurring in 62% of patients within six months of treatment (acute) and 91% thereafter (late), as classified by a common classification scheme (22,23). This scheme classifies acute radiation pneumonitis into consolidative or ground-glass opacity changes, which can further be subdivided into diffuse (>5 cm) or patchy (≤5 cm). Late radiation fibrosis can be categorized into modified conventional, mass-like, or scar-like patterns. Although this classification scheme is used to categorize radiological changes following SABR, it is not used to distinguish recurrence from fibrosis. Morphologic patterns of fibrosis can also vary with treatment type; patients that underwent arc-based SABR had a predicted probability of a modified conventional pattern of 96.3% versus 68.9% for those who underwent fixed-beam treatment (28). Although such radiologic lung injury occurs in nearly all patients by two years (22), only a small minority of patients develop clinical symptoms.

Against this background of asymptomatic radiation-induced lung injury, accurate assessment of local recurrence is of paramount importance. Misclassification of a recurrence as "benign fibrosis" can result in a missed window of opportunity for curative-intent salvage treatment. Conversely, misclassification of fibrosis as a recurrence may lead to unnecessary interventions, such as biopsy, imaging, chemotherapy, and even surgery, exposing patients to unnecessary risks and morbidity (27,29-32). The ability to accurately assess response is particularly important in light of the changing practice patterns for early stage NSCLC. As a growing number of patients are being treated by SABR (5), this clinical scenario will become more common. The treatment of a fitter patient population may result in a larger proportion of patients who are candidates for salvage treatment in the case of recurrence. Finally, since recent data on potentially operable SABR patients suggest that failure may be higher than in the inoperable SABR cohort [with two-year lobar failure rates in one recent multicenter study (defined as recurrence anywhere in the irradiated lobe) as high as 19.2% (19)], accurate distinction between recurrence and fibrosis to permit early salvage is a pressing clinical problem.

Distinguishing a recurrent tumor from fibrotic lung changes on CT can be challenging for several reasons (Figure 1). Both radiation-induced lung injury and recurrent disease follow a similar temporal course, with lung fibrosis continuing to evolve two years after treatment, during which time, the majority of local recurrences occur (22,33). In contrast to lung injury following traditional 3D-CRT, which was often characterized by straight edges that conform to treatment portals (34) (Figure 2), the pattern of lung injury on CT following SABR can be mass-like, due to the conformal nature of SABR (22,31,35). Fibrosis may even appear on CT as an enlarging density and therefore can the mimic the growth of a local recurrence (31).

Current clinical approach for assessing response

Current recommendations for imaging follow-up after SABR are generally based on retrospective evidence and expert opinion, rather than randomized data. Such follow-up serves three major goals: detection of local recurrence, detection of regional recurrence that may be amenable to salvage, and detection of new primary lung tumors, which occur at a rate of 2-10% per person-year (33,36). Based on the results of the National Lung Screening Trial (37), the American Association for Thoracic Surgery guidelines recommends four years of CT follow-up for patients who have undergone treatment for lung cancer and are eligible for additional treatment (38).

Tumor response assessment following definitive treatment is typically categorized according to Response Evaluation Criteria in Solid Tumors (RECIST) 1.1 criteria (39) as complete

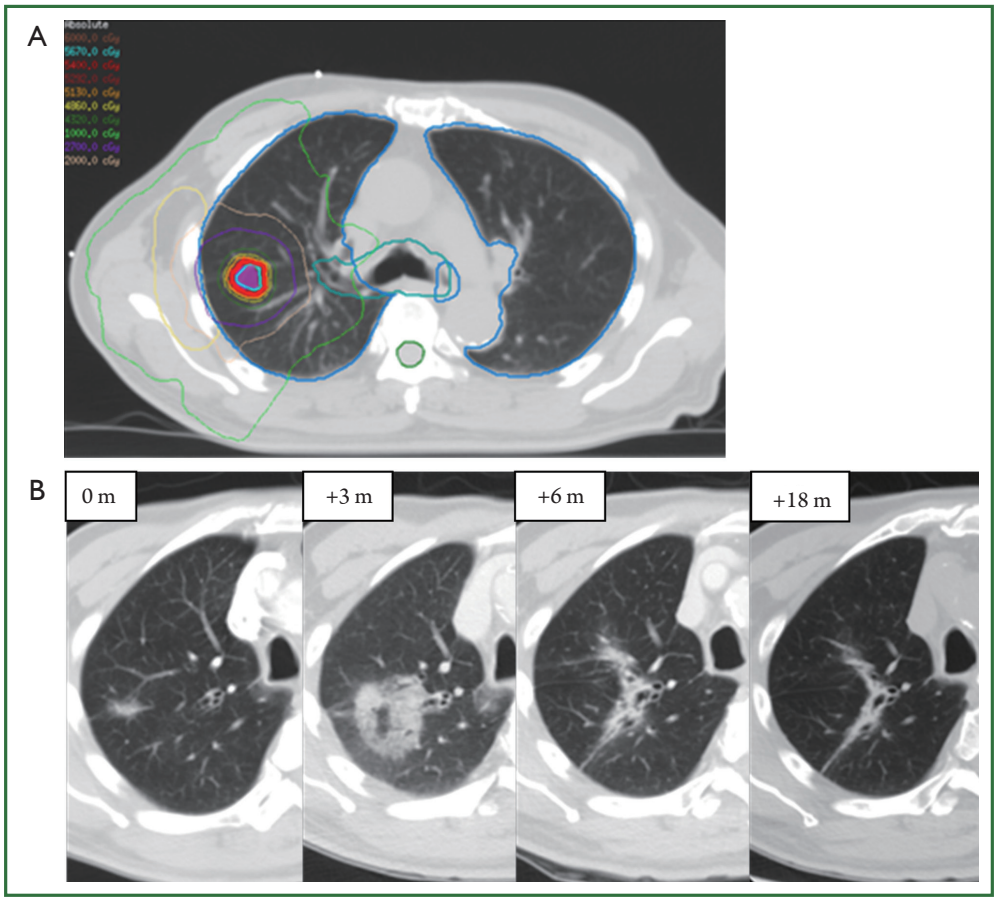

Figure 1. Radiological changes following SABR for an 85-year-old gentleman with biopsy proven adenocarcinoma. This patient received 54 Gy in 3 fractions with the treatment plan shown in (A). Radiological changes are seen (B) where 0 m indicates the pre-treatment lesion measuring 2.0 cm. At 3 months post-SABR, further enlargement of a ground-glass semi-solid opacity measuring 4.3 cm and at 6 months there is interval reduction in size and a decrease in ground-glass opacity, with ongoing reduction in size by 18 months.

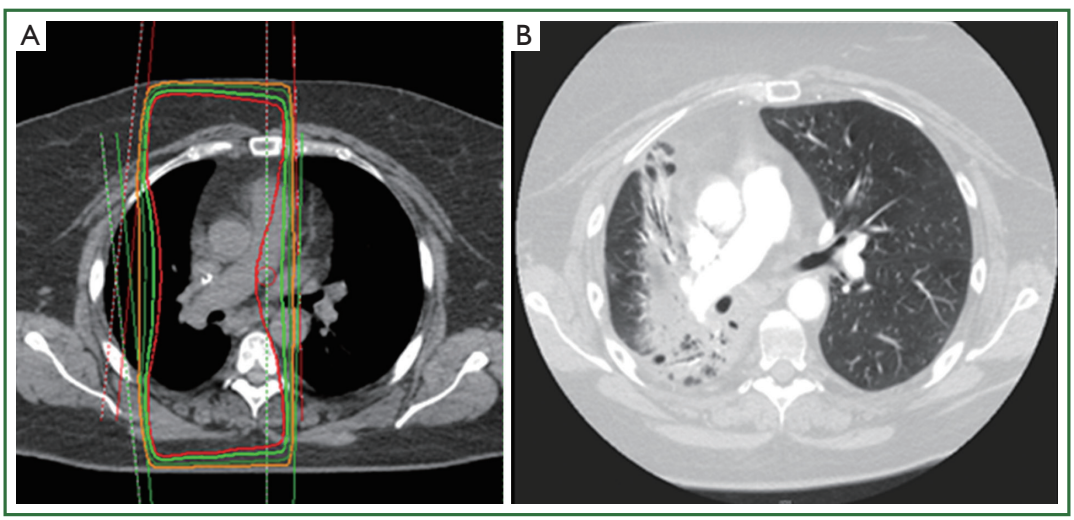

Figure 2. Radiation induced lung injury following a traditional anterior/posterior parallel opposed pair (treatment plan shown in Box A); (B) The resulting benign injury conforms to the treatment portals and is easily distinguished by a straight line.

Table 1. Selected studies using FDG-PET for detecting recurrence following SABR.

Study	Number of patients	Number of recurrences [proportion pathology proven %]	SUV_{max} cutoff	Sensitivity (%)	Specificity (%)	Definition of local recurrence if not biopsied
Essler, *et al.* (50)	29	6 [NR]	5.48	NR	NR	Increase in tumor volume of more than 25% on CT, accompanied by metabolic activity in FDG-PET
Bollineni, *et al.* (49)	132	6 [50]	5.0	NR	NR	Based on growth by more than 20% of the tumor diameter compared with the pretreatment
Zhang, *et al.* (47)	128	9 [78]	5.0	100	91	PET/CT
Takeda *et al.* (48)	154	17 [18]	3.2 (early) 4.2 (late)	100	96-98	Increase in the cross-sectional tumor size of >25% on successive CT scans at least three times over a 6-month period

NR, not reported.

Table 2. High-risk features for recurrence on CT. Data from reference (51).

High-risk feature	Sensitivity (%)	Specificity (%)
Enlarging opacity	92	67
Sequential enlargement	67	100
Enlargement after 12 months	100	83
Bulging margin	83	83
Linear margin disappearance	42	100
Loss air bronchogram	67	96
Cranio-caudal growth of ≥5 mm and ≥20%	92	83

(disappearance of the target), partial (≥30% decrease), stable disease, or progression (≥20% increase) according to the diameter of the target tumor. However, RECIST 1.1 has limited use in the post-SABR lung setting, since the target lesion may actually represent lung fibrosis, and response may be mis-categorised (11,40). Re-evaluation of RECIST 1.1 has been proposed (41).

Although FDG-PET scans are recommended in lung cancer diagnosis and re-staging (42), functional imaging currently has a limited role in the evaluation of tumor response and detection of local recurrence. Lung injury following ablative radiation doses can commonly result in a metabolically active FDG-avid lesion, which may rise transiently immediately post-SABR and persist after 12 months (43-45). False-positive PET SUV_{max} readings as high as 7.0 have been reported (27,46). Most evidence supports a SUV_{max} of approximately 5.0 as a clinically useful threshold for the distinction between recurrence and fibrosis (47-50). Table 1 summarizes selected studies using FDG-PET to assess treatment response post-SABR.

Following SABR, recommended surveillance for patients eligible for salvage treatment is routine CT imaging, often at 3-6-month intervals in the first year, then annually thereafter (8,38). A systematic review of the literature on the role of imaging in discriminating recurrence from fibrosis provides structured recommendations based on the available evidence, citing high-risk features (HRFs, Table 2) on CT (31,35,52) and specific SUV_{max} thresholds to estimate the probability of recurrence and appropriate investigations into "no-risk" "low-risk" and "high-risk" categories (23). The clinical performance of the HRFs was validated by a blinded assessment of matched CT datasets from pathology-proven recurrences and non-recurrences (51). The concurrent presence of ≥3 HRFs provides a useful cutoff (sensitivity and specificity both >90%) for detection of recurrence.

There are several advantages to the use of CT, rather than routine functional imaging, in assessment of response post-SABR. In contrast to FDG-PET imaging, CT is more accessible and inexpensive, does not rely on isotopes with short half-lives, and

is already part of standard-of-care follow-up for patients who have received curative treatment for early-stage lung cancer, and who are eligible for salvage. Importantly, standardization of CT across centres is much less complex than standardization of PET/CT. Lack of PET/CT standardization can be an important confounder: measured SUVs can be affected by multiple factors, including technical, physical, and biologic (53). In order to generalize PET/CT findings, minimum performance or harmonizing standards are needed for many factors including uptake period, patient motion, inflammation, blood glucose level correction, as well as scan acquisition and reconstruction parameters. Standard machine settings and reconstruction algorithms are widely available for CT imaging of the chest, increasing the generalizability of any follow-up recommendations. As such, new algorithms for early detection of recurrence based on standard-of-care CT imaging could be easily integrated into current clinical practice. However, novel imaging techniques must move beyond qualitative image analysis and simple RECIST measurements.

Quantitative image feature analysis

In contrast to qualitative image assessment described above, quantitative image feature analysis extracts measurable information from within an image, such as intensities or densities, shape or morphology, or texture. Intensity refers the brightness of an individual voxel; in CT imaging this can also be described as density and is quantified in Hounsfield Units (HUs). HUs measure the attenuation of a material relative to water (HU =0). The shape or morphology of a region describes the geometry of the external boundary. "CT image texture" is a set of more complex measurements which describe local brightness variation or the spatial arrangement of intensities in an image (54,55).

Image feature analysis has emerging roles in general medicine and oncology. Numerous imaging modalities can be used for quantitative image analysis at different body sites, including CT, magnetic resonance imaging (MRI), ultrasound, and mammography (56,57). Applications in oncology include the computer-aided detection or diagnosis of diseases such as breast and bladder cancer (56,57). Texture analysis of the liver has suggested that texture parameters may distinguish high-risk from low-risk colorectal cancer patients (58). Texture analysis on MRI, CT, and PET has been able to diagnose and characterize tumor heterogeneity for several tumor types and is showing promise in response assessment and as a predictive biomarker (59,60). In the thorax, the use of quantitative image feature analysis on CT has been widely investigated in many benign diseases, including characterizing pulmonary infections as well as varying benign lung disease patterns (61-63). Texture analysis, specifically the product of tumor uniformity and gray-level, has also been correlated with tumor response following chemotherapy in advanced stage NSCLC (64).

Quantitative image analysis workflow

Figure 3 demonstrates the typical workflow for quantitative image feature analysis. In general, image acquisition should be standardized to minimize any variability between scanners, imaging parameters, or reconstruction techniques. Standardization includes the use of the same scan protocol for imaging acquisition, with consistencies in settings such as kV, mAs, slice collimation, and slice thickness. Breathing instructions and the use of intravenous contrast should also be consistent across all patients, although patients with contra-indications to contrast injection must be noted and studies analyzing the effect of contrast on image feature analysis should be performed. Reconstruction kernels or filters are used to determine image quality of a CT scan and are chosen based on the intended clinical application of the scan. Such decisions are a compromise between spatial resolution and noise, and depending on the organ being scanned, may require a smoother image with less noise or a sharper image with higher noise. Reconstruction kernels should also be consistent across all images and a higher sharpness thorax kernel should be used when available. However, optimal scan parameters and reconstruction kernels must be investigated for the effect of variations among these settings on quantitative image feature analysis.

Image feature analysis can be performed on any region of interest (ROI), such as tumor, normal lung, or fibrotic regions; such ROIs can be selected by means of manual, semi-automated, or fully-automated methods. A manual method involves delineation of an ROI by an investigator on each individual slice using imaging software. Manual methods do not require specialized algorithms, but can be tedious and time consuming, and are subject to intra- and inter-observer variability (65). A semi-automated method requires a smaller amount of user input, and may require a user to initialize the segmentation by selecting a point or ROI. A fully automated approach requires no user interaction or input and the image is automatically segmented based on a series of predetermined parameters. This makes a fully automated approach quick and reproducible; however the lack of user input or knowledge can be an issue in terms of reliability. Therefore, semi-automated approaches to segmentation have become increasingly popular as they are reproducible, fast, and require minimal user input or knowledge (66).

After ROIs are delineated, quantitative measures can then

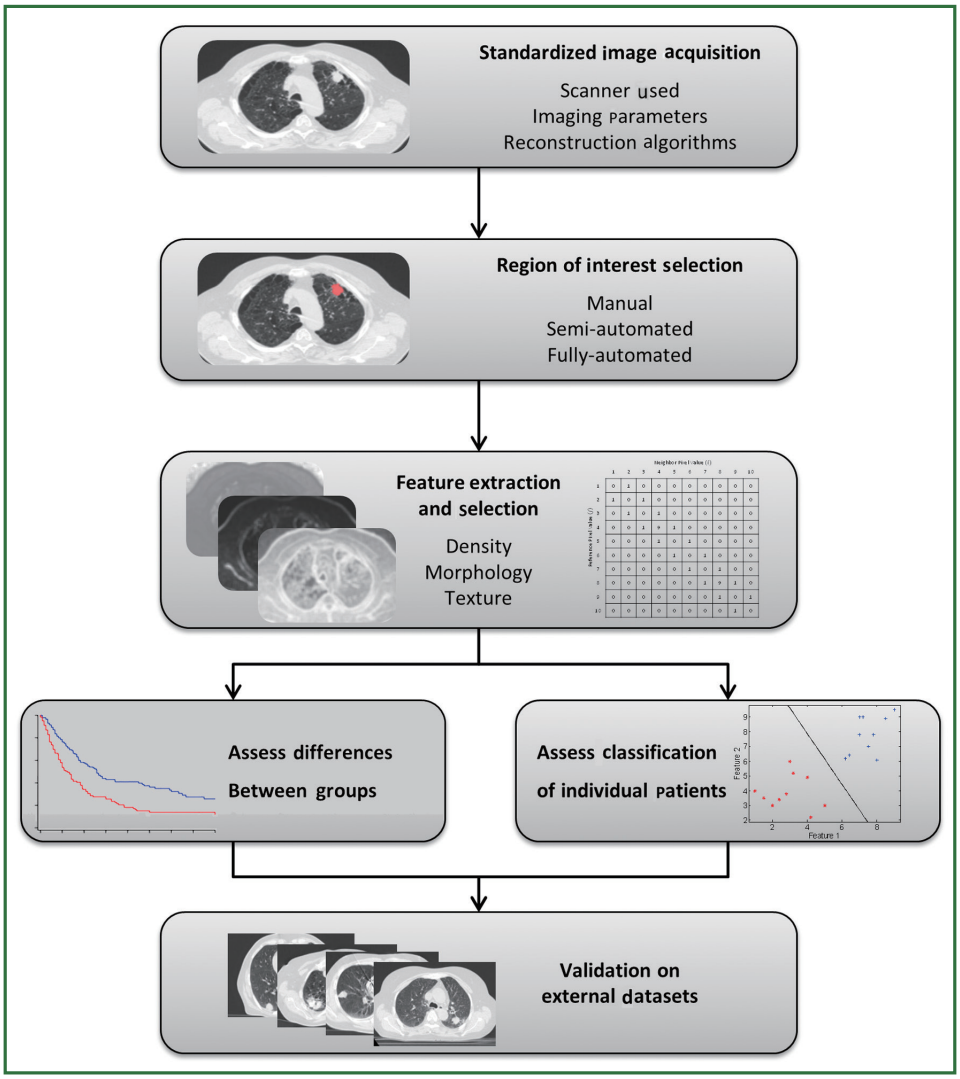

Figure 3. Typical workflow for image feature analysis.

be extracted including measures such as density, morphology, or texture, and these measures can be evaluated as predictive or prognostic biomarkers. Extracted measures can be calculated with a variety of input parameters and settings specific to each case. Such measures range from simple first-order assessments such as the mean HU density within a region, to complex measures of the spatial relationship of voxel intensities, for example analyzing neighboring voxels of varying distances apart.

Optimal features or sets of features for predictive or prognostic biomarkers must be determined and validated through training and testing on multiple data sets. This can include analyzing individual features alone or a combination of these features together. Due to the large number of metrics available as well as the large number of possible combinations of these metrics, the high-risk of type I error must be recognized when comparisons and cross-validations are performed. As a result, initial exploratory studies must be considered hypothesis-generating, and validation on external datasets is crucial.

Common metrics used for image feature analysis

Image feature analysis metrics can be defined as first-order, second-order, and third-order. First-order image appearance features measure the global appearance of a ROI and do not take into consideration relationships between adjacent voxels. A common example includes the mean density based on CT HU. The standard deviation of density can be used as a first-order texture feature, which shows the global variability of densities

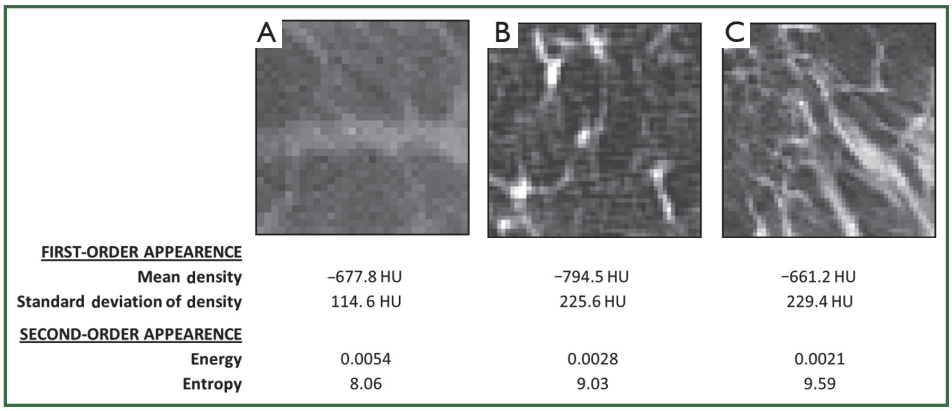

Figure 4. Sample lung images showing the variations in two first-order appearance measures [mean density and standard deviation of density (first-order texture analysis)] and two second-order appearance measures, energy and entropy. (A) and (C) have similar mean densities, but are better differentiated by the first- and second-order texture measures. (B) and (C) have similar first-order texture values, but are better differentiated by the second-order measures.

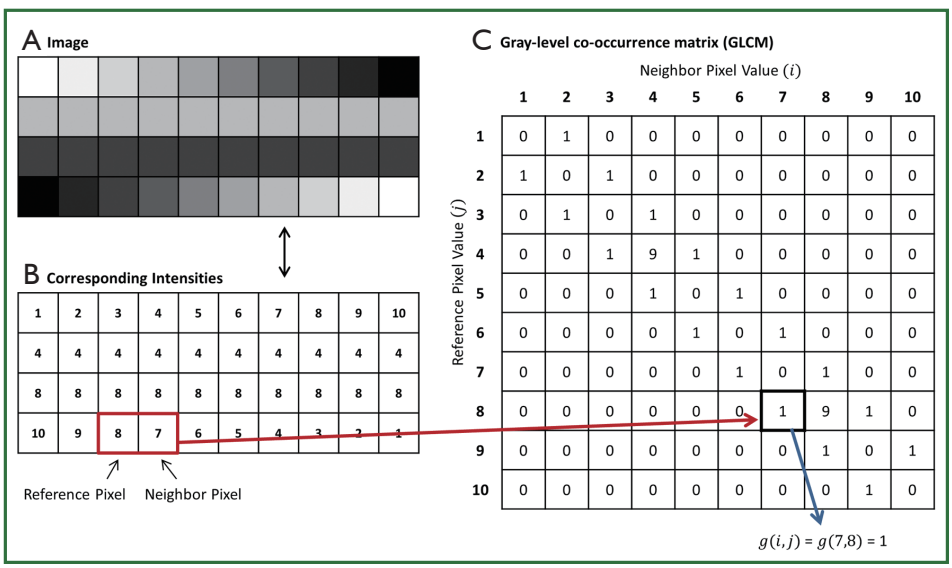

Figure 5. A sample image (A) with its corresponding numerical intensity values (B). The gray-level co-occurrence matrix (GLCM) for this image can be seen in (C), with the pixel relationship for analysis being one voxel to the right, as indicated by the reference and neighbor pixel.

within a region (Figure 4). Second-order appearance measures characterize the intensity relationships between voxels pairs in an image, whereas third-order measures (which are less commonly used) consider the spatial relationship of three or more voxels in an image. Extraction of second and third-order texture features can be performed in many ways, including statistical methods, structural methods, model-based methods, and transform-based methods (67).

Statistical texture analysis is the most frequently cited method of texture analysis. This approach describes texture through high-order statistics of an image intensity histogram (67). This analysis typically assesses neighboring voxel pairs; however it can be done with multiple spatial directions and distances. Second-order statistical texture features are typically computed with the use of a grey-level co-occurrence matrix (GLCM). As shown in Figure 5, A GLCM is a square two-dimensional matrix g, in which the row and columns correspond to image intensity values. Each element in the matrix $g(i,j)$ contains a non-negative integer corresponding to the number of voxel pairs whose intensity values are i and j. A variety of texture measures can be calculated from the GLCM, such as energy, entropy, inverse difference moment

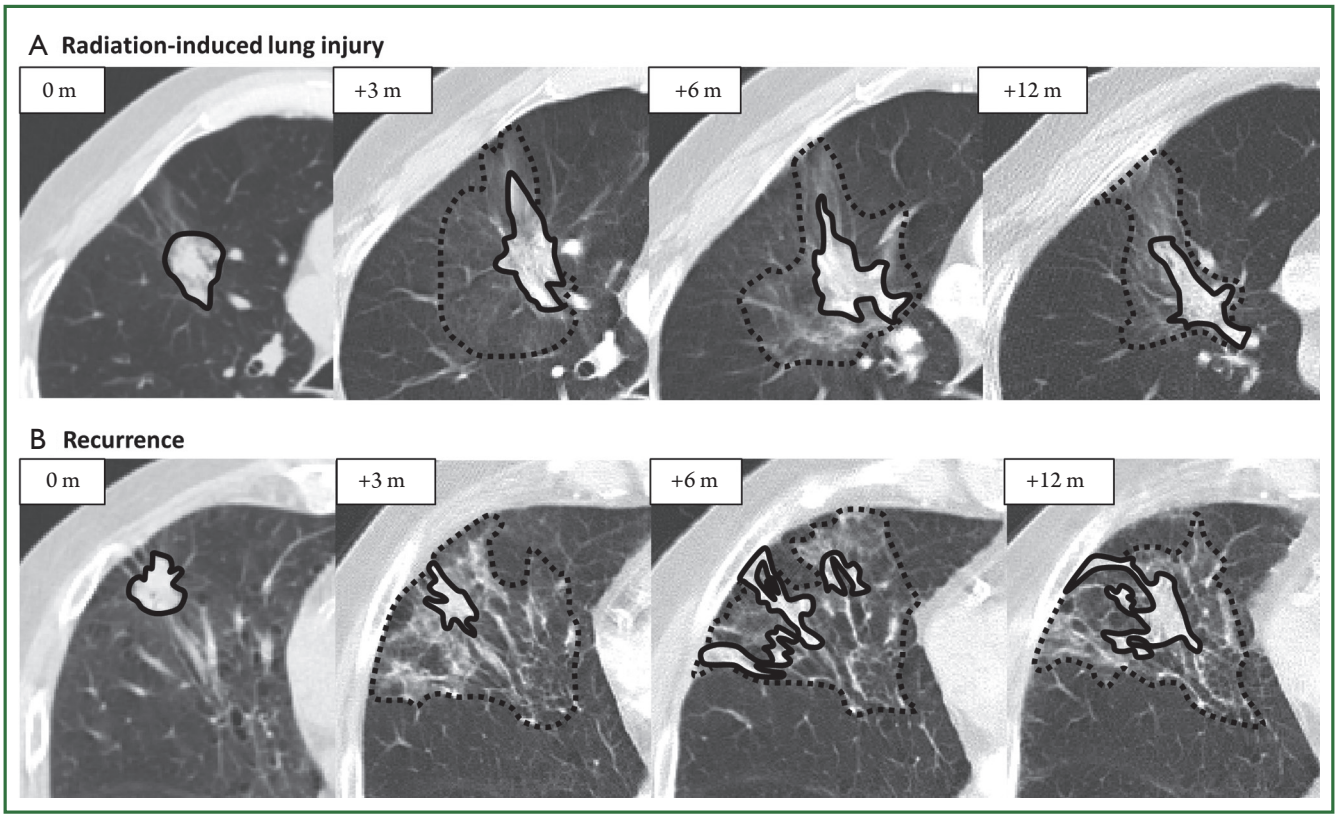

Figure 6. Post-SABR consolidative and ground-glass opacity findings throughout follow-up for a patient with radiation-induced lung injury (A) and recurrence (B). The zero-month (0 m) time point indicates the pre-treatment lesion. The solid lines enclose consolidative regions and the dashed lines enclose ground-glass opacity regions.

(IDM), inertia, cluster shade, and cluster prominence (68-70). In general, energy and entropy measure the orderliness of the GLCM, or the homogeneity of the image. IDM and inertia measure the contrast of the image, and cluster shade and cluster prominence measure the symmetry of an image.

An example of images with their corresponding first-order and second-order appearance measures is seen in Figure 4. The variation in the number and distribution of vessels in the image results in differences in feature measurements. For example, Figure 4A and C have similar mean densities but are better differentiated by the texture measures, both first-order and second-order. Figure 4B and C have similar first-order texture feature measurements but are differentiated by the second-order measures of energy and entropy. Each measure can extract specific information from the image, and overall first-order measures are less sensitive to spatial variations in intensities whereas second-order appearance measures are taking neighboring voxels into account and are therefore sensitive to the relationship of voxels.

Image feature analysis post-SABR

Several studies have examined simple dose-response relationships of HU changes following SABR. Increasing densities on CT post-SABR are seen with larger planning target volumes and longer time post-SABR, and these are most evident in regions receiving doses greater than 20 Gy (24). Density changes post-SABR have also been shown to linearly increase to doses of 35-40 Gy and then plateau thereafter (24,71). The spatial location of fibrosis following SABR is on average 2.6 cm from the gross tumor volume (GTV) position, although displacement of the fibrotic changes of >5 cm can also be observed (72).

Quantitative image analysis has been investigated for distinguishing RILI and recurrence following SABR (Figure 6). A preliminary study of 13 RILI lesions and 11 recurrent lesions (8 biopsy proven) suggested that first-order appearance measures could significantly distinguish RILI and recurrence patient groups at 9 months following treatment, with recurrence patients having significantly brighter consolidative changes (73).

The standard deviation of densities within regions of GGO (first-order texture analysis) could also distinguish the groups at nine months, with recurrence patients having a larger standard deviation (variability) of densities. This indicates that these patients have a more variegated texture within the GGO, as seen in Figure 4. In contrast, size measures (RECIST or 3D volume) could not differentiate the groups until 15 months post-treatment. A preliminary study of predictive abilities of these measures has shown that the first-order texture analysis within the GGO was the best predictor of recurrence at nine months post-SABR with accuracies of 74% (74).

Further investigation has evaluated texture changes in the immediate post-SABR period. At 2-5 months post-SABR, preliminary analysis suggests that the basic measure of ground-glass texture alone can predict recurrence with 81% accuracy (75). Several second-order texture features have also shown promise, including energy and entropy, with leave-one-out cross validation accuracies of 81% and AUCs of 0.79-0.81 (75). Patients with recurrence had significantly higher entropy and lower energy values. In contrast, traditional measures of response such as RECIST performed inferiorly, with accuracy of 61% and an AUC of 0.72. These results suggest that early quantitative appearance changes may precede any changes in size, and as such may serve as early biomarkers of recurrence in individual patients. Quantitative image analysis allows for maximal information to be obtained from images already being performed in clinical practice, and can easily be translated into a useful clinical tool to aid in treatment response assessment. Further quantitative metrics, including additional second-order textural features and shape analysis, should be investigated and validated for early prediction of recurrence following SABR.

Future directions and potential pitfalls

Novel imaging modalities may allow for better assessment of treatment responses following SABR or HFRT. In addition to standard FDG-PET reporting SUV_{max} values, functional imaging with additional metrics such as metabolic tumor burden markers may show improvement for assessing response. Preliminary studies have investigated using pre-treatment measures such as metabolic tumor volume and total lesion glycolysis for assessing clinical outcomes after SABR, however further studies with larger samples and follow-up periods are needed (76). Additional PET tracers such as 18-fluoroazomycin-arabinoside (FAZA) and 18F-fluoromisonidazole (F-MISO) are used for imaging hypoxia in head and neck cancers (77,78) and could also be investigated for assessing response following HFRT.

Perfusion imaging, such as dynamic-contrast-enhanced-CT (DCE-CT) or MRI (DCE-MRI) characterizes vascular properties of a tissue and can quantitatively map their spatial distributions. Measures such as blood volume, blood flow, permeability, and mean transit time can be calculated after administration of a contrast agent. Both DCE-CT and DCE-MRI have shown promise as prognostic or predictive biomarkers in oncology, and their value in assessing response after SABR warrants investigation (79,80).

Several potential pitfalls must be considered when evaluating novel imaging modalities for response assessment. First, the gold-standard definition of "recurrence" varies across studies, and many studies use imaging-based definitions of recurrence, rather than pathologic confirmation. Such imaging-based definitions of the endpoint may introduce substantial bias and create a self-fulfilling prophesy: if imaging features are used to define "recurrence" (e.g., sequential growth of lesion) and then the same features are assessed to predict these "recurrences", their performance may be artificially inflated. The majority of studies include only a small number of biopsy-proven recurrences, with remainder of patients defined as recurrence based on an increase in tumor size on successive CT scans (48,49,81). Many also use a modified progression criterion of two consecutive enlargements on CT to define recurrence, which hampers response assessment at an early time point, and suggesting that and that the usefulness of PET is limited. Since recurrences are uncommon after SABR, large databases are required to have sufficient events for analysis, and any new promising markers require robust external validation, since the chances of type I error are high when multiple features are being assessed. Variations in standardization of imaging protocols in both CT and PET studies must be assessed for their impact on predictive ability. Finally, post-SABR surgical studies, including registration of digitized histology to CT, would be valuable for correlating imaging findings at the voxel level with true pathologic outcome.

Conclusions

Distinguishing recurrence from fibrosis following SABR for early-stage lung cancer is expected to become an increasingly common clinical problem. Although recommendations exist for CT- and PET/CT-based follow-up after SABR, better metrics are required for early detection of recurrence, to allow for salvage, and to avoid unnecessary investigations in patients with benign radiation-induced lung injury. Promising new techniques may involve more robust analysis of currently-obtained imaging, such as CT texture analysis, or introduction of novel imaging modalities into routine clinical practice. Large imaging datasets are required for assessment and subsequent independent

validation of novel new imaging biomarkers.

Acknowledgements

This project is supported by a research grant from the National Sciences and Engineering Research Council. Dr. Palma is a recipient of research funding from the Ontario Institute for Cancer Research. Dr. Ward acknowledges the support of the Cancer Care Ontario Research Chairs program. The VU university medical center has a research agreement with Varian Medical Systems, Inc.
Disclosure: The authors DP, SM, SS and AW hold a provisional patent regarding advanced CT image analysis for assessment of response after lung cancer radiotherapy. The authors declare no additional conflict of interest.

References

1. Soliman H, Cheung P, Yeung L, et al. Accelerated hypofractionated radiotherapy for early-stage non-small-cell lung cancer: long-term results. Int J Radiat Oncol Biol Phys 2011;79:459-65.
2. Bogart JA, Hodgson L, Seagren SL, et al. Phase I study of accelerated conformal radiotherapy for stage I non-small-cell lung cancer in patients with pulmonary dysfunction: CALGB 39904. J Clin Oncol 2010;28:202-6.
3. Smith SL, Palma D, Parhar T, et al. Inoperable early stage non-small cell lung cancer: comorbidity, patterns of care and survival. Lung Cancer 2011;72:39-44.
4. Onishi H, Shirato H, Nagata Y, et al. Hypofractionated stereotactic radiotherapy (HypoFXSRT) for stage I non-small cell lung cancer: updated results of 257 patients in a Japanese multi-institutional study. J Thorac Oncol 2007;2:S94-100.
5. Pan H, Simpson DR, Mell LK, et al. A survey of stereotactic body radiotherapy use in the United States. Cancer 2011;117:4566-72.
6. Palma DA, Senan S. Early-stage non-small cell lung cancer in elderly patients: should stereotactic radiation therapy be the standard of care? Int J Radiat Oncol Biol Phys 2012;84:1058-9.
7. Palma D, Senan S. Stereotactic radiation therapy: changing treatment paradigms for stage I nonsmall cell lung cancer. Curr Opin Oncol 2011;23:133-9.
8. Vansteenkiste J, De Ruysscher D, Eberhardt WE, et al. Early and locally advanced non-small-cell lung cancer (NSCLC): ESMO Clinical Practice Guidelines for diagnosis, treatment and follow-up. Ann Oncol 2013;24 Suppl 6:vi89-98.
9. Palma D, Visser O, Lagerwaard FJ, et al. Impact of introducing stereotactic lung radiotherapy for elderly patients with stage I non-small-cell lung cancer: a population-based time-trend analysis. J Clin Oncol 2010;28:5153-9.
10. Haasbeek CJ, Palma D, Visser O, et al. Early-stage lung cancer in elderly patients: a population-based study of changes in treatment patterns and survival in the Netherlands. Ann Oncol 2012;23:2743-7.
11. Senan S, Palma DA, Lagerwaard FJ. Stereotactic ablative radiotherapy for stage I NSCLC: Recent advances and controversies. J Thorac Dis 2011;3:189-96.
12. Shirvani SM, Jiang J, Chang JY, et al. Comparative effectiveness of 5 treatment strategies for early-stage non-small cell lung cancer in the elderly. Int J Radiat Oncol Biol Phys 2012;84:1060-70.
13. Nguyen NP, Garland L, Welsh J, et al. Can stereotactic fractionated radiation therapy become the standard of care for early stage non-small cell lung carcinoma. Cancer Treat Rev 2008;34:719-27.
14. Timmerman R, Paulus R, Galvin J, et al. Stereotactic body radiation therapy for inoperable early stage lung cancer. JAMA 2010;303:1070-6.
15. Louie AV, Rodrigues G, Hannouf M, et al. Stereotactic body radiotherapy versus surgery for medically operable Stage I non-small-cell lung cancer: a Markov model-based decision analysis. Int J Radiat Oncol Biol Phys 2011;81:964-73.
16. Varlotto J, Fakiris A, Flickinger J, et al. Matched-pair and propensity score comparisons of outcomes of patients with clinical stage I non-small cell lung cancer treated with resection or stereotactic radiosurgery. Cancer 2013;119:2683-91.
17. Verstegen NE, Oosterhuis JW, Palma DA, et al. Stage I-II non-small-cell lung cancer treated using either stereotactic ablative radiotherapy (SABR) or lobectomy by video-assisted thoracoscopic surgery (VATS): outcomes of a propensity score-matched analysis. Ann Oncol 2013;24:1543-8.
18. Palma D, Lagerwaard F, Rodrigues G, et al. Curative treatment of Stage I non-small-cell lung cancer in patients with severe COPD: stereotactic radiotherapy outcomes and systematic review. Int J Radiat Oncol Biol Phys 2012;82:1149-56.
19. Timmerman RD, Paulus R, Pass HI, et al. RTOG 0618: Stereotactic body radiation therapy (SBRT) to treat operable early-stage lung cancer patients (Abstract 7523). American Society of Clinical Oncology 2013 meeting.
20. Nagata Y, Hiraoka M, Shibata T, et al. A Phase II Trial of Stereotactic Body Radiation Therapy for Operable T1N0M0 Non-small Cell Lung Cancer. Japan Clinical Oncology Group (JCOG0403). Int J Radiat Oncol Biol Phys 2010;78:S27.
21. Cheung P, Faria S, Ahmed S, et al. A phase II study of accelerated hypofractionated 3-dimensional conformal radiotherapy for inoperable T1-3 N0 M0 non-small cell lung cancer: NCIC CTG BR.25. Canadian Assoc Rad Oncol 2012:abstr 171.
22. Dahele M, Palma D, Lagerwaard F, et al. Radiological changes after stereotactic radiotherapy for stage I lung cancer. J Thorac Oncol 2011;6:1221-8.
23. Huang K, Dahele M, Senan S, et al. Radiographic changes after lung stereotactic ablative radiotherapy (SABR)--can we distinguish recurrence from fibrosis? A systematic review of the literature. Radiother Oncol 2012;102:335-42.
24. Palma DA, van Sörnsen de Koste J, Verbakel WF, et al. Lung density changes after stereotactic radiotherapy: a quantitative analysis in 50 patients. Int J Radiat Oncol Biol Phys 2011;81:974-8.

25. Kickingereder P, Dorn F, Blau T, et al. Differentiation of local tumor recurrence from radiation-induced changes after stereotactic radiosurgery for treatment of brain metastasis: case report and review of the literature. Radiat Oncol 2013;8:52.
26. Pan CC, Kavanagh BD, Dawson LA, et al. Radiation-associated liver injury. Int J Radiat Oncol Biol Phys 2010;76:S94-100.
27. Singhvi M, Lee P. Illustrative cases of false positive biopsies after stereotactic body radiation therapy for lung cancer based on abnormal FDG-PET-CT imaging. BMJ Case Rep 2013;2013. pii: bcr2012007967.
28. Senthi S, Dahele M, van de Ven PM, et al. Late radiologic changes after stereotactic ablative radiotherapy for early stage lung cancer: A comparison of fixed-beam versus arc delivery techniques. Radiother Oncol 2013;109:77-81.
29. Wiener RS, Schwartz LM, Woloshin S, et al. Population-based risk for complications after transthoracic needle lung biopsy of a pulmonary nodule: an analysis of discharge records. Ann Intern Med 2011;155:137-44.
30. Gupta S, Wallace MJ, Cardella JF, et al. Quality improvement guidelines for percutaneous needle biopsy. J Vasc Interv Radiol 2010;21:969-75.
31. Takeda A, Kunieda E, Takeda T, et al. Possible misinterpretation of demarcated solid patterns of radiation fibrosis on CT scans as tumor recurrence in patients receiving hypofractionated stereotactic radiotherapy for lung cancer. Int J Radiat Oncol Biol Phys 2008;70:1057-65.
32. Stauder MC, Rooney JW, Neben-Wittich MA, et al. Late tumor pseudoprogression followed by complete remission after lung stereotactic ablative radiotherapy. Radiat Oncol 2013;8:167.
33. Senthi S, Lagerwaard FJ, Haasbeek CJ, et al. Patterns of disease recurrence after stereotactic ablative radiotherapy for early stage non-small-cell lung cancer: a retrospective analysis. Lancet Oncol 2012;13:802-9.
34. Libshitz HI, Shuman LS. Radiation-induced pulmonary change: CT findings. J Comput Assist Tomogr 1984;8:15-9.
35. Matsuo Y, Nagata Y, Mizowaki T, et al. Evaluation of mass-like consolidation after stereotactic body radiation therapy for lung tumors. Int J Clin Oncol 2007;12:356-62.
36. Lou F, Huang J, Sima CS, et al. Patterns of recurrence and second primary lung cancer in early-stage lung cancer survivors followed with routine computed tomography surveillance. J Thorac Cardiovasc Surg 2013;145:75-81; discussion 81-2.
37. National Lung Screening Trial Research Team, Aberle DR, Adams AM, et al. Reduced lung-cancer mortality with low-dose computed tomographic screening. N Engl J Med 2011;365:395-409.
38. Jaklitsch MT, Jacobson FL, Austin JH, et al. The American Association for Thoracic Surgery guidelines for lung cancer screening using low-dose computed tomography scans for lung cancer survivors and other high-risk groups. J Thorac Cardiovasc Surg 2012;144:33-8.
39. Eisenhauer EA, Therasse P, Bogaerts J, et al. New response evaluation criteria in solid tumours: revised RECIST guideline (version 1.1). Eur J Cancer 2009;45:228-47.
40. Dunlap NE, Yang W, McIntosh A, et al. Computed tomography-based anatomic assessment overestimates local tumor recurrence in patients with mass-like consolidation after stereotactic body radiotherapy for early-stage non-small cell lung cancer. Int J Radiat Oncol Biol Phys 2012;84:1071-7.
41. Oxnard GR, Morris MJ, Hodi FS, et al. When progressive disease does not mean treatment failure: reconsidering the criteria for progression. J Natl Cancer Inst 2012;104:1534-41.
42. Donington J, Ferguson M, Mazzone P, et al. American College of Chest Physicians and Society of Thoracic Surgeons consensus statement for evaluation and management for high-risk patients with stage I non-small cell lung cancer. Chest 2012;142:1620-35.
43. Fuss M. Strategies of assessing and quantifying radiation treatment metabolic tumor response using F18 FDG Positron Emission Tomography (PET). Acta Oncol 2010;49:948-55.
44. Henderson MA, Hoopes DJ, Fletcher JW, et al. A pilot trial of serial 18F-fluorodeoxyglucose positron emission tomography in patients with medically inoperable stage I non-small-cell lung cancer treated with hypofractionated stereotactic body radiotherapy. Int J Radiat Oncol Biol Phys 2010;76:789-95.
45. Matsuo Y, Nakamoto Y, Nagata Y, et al. Characterization of FDG-PET images after stereotactic body radiation therapy for lung cancer. Radiother Oncol 2010;97:200-4.
46. Feigenberg S, Yu JQM, Eade TN, et al. FDG PET response by 3 months following stereotactic body radiotherapy for non-small cell lung cancer may be an early surrogate of local failure [abstract]. Int J Radiat Oncol Biol Phys 2007;69:S479-80.
47. Zhang X, Liu H, Balter P, et al. Positron emission tomography for assessing local failure after stereotactic body radiotherapy for non-small-cell lung cancer. Int J Radiat Oncol Biol Phys 2012;83:1558-65.
48. Takeda A, Kunieda E, Fujii H, et al. Evaluation for local failure by 18F-FDG PET/CT in comparison with CT findings after stereotactic body radiotherapy (SBRT) for localized non-small-cell lung cancer. Lung Cancer 2013;79:248-53.
49. Bollineni VR, Widder J, Pruim J, et al. Residual ^{18}F-FDG-PET uptake 12 weeks after stereotactic ablative radiotherapy for stage I non-small-cell lung cancer predicts local control. Int J Radiat Oncol Biol Phys 2012;83:e551-5.
50. Essler M, Wantke J, Mayer B, et al. Positron-emission tomography CT to identify local recurrence in stage I lung cancer patients 1 year after stereotactic body radiation therapy. Strahlenther Onkol 2013;189:495-501.
51. Huang K, Senthi S, Palma DA, et al. High-risk CT features for detection of local recurrence after stereotactic ablative radiotherapy for lung cancer. Radiother Oncol 2013;109:51-7.
52. Kato S, Nambu A, Onishi H, et al. Computed tomography appearances of local recurrence after stereotactic body radiation therapy for stage I non-small-cell lung carcinoma. Jpn J Radiol 2010;28:259-65.
53. Boellaard R. Need for standardization of 18F-FDG PET/CT for treatment response assessments. J Nucl Med 2011;52 Suppl 2:93S-100S.
54. Russ JC. The Image Processing Handbook. Fifth Edition. Taylor & Francis, 2006.

55. IEEE Standard Glossary of Image Processing and Pattern Recognition Terminology. IEEE Std 6104-1990 1990:0_1.
56. Shi Z, Yang Z, Zhang G, et al. Characterization of texture features of bladder carcinoma and the bladder wall on MRI: initial experience. Acad Radiol 2013;20:930-8.
57. Jalalian A, Mashohor SB, Mahmud HR, et al. Computer-aided detection/diagnosis of breast cancer in mammography and ultrasound: a review. Clin Imaging 2013;37:420-6.
58. Ganeshan B, Burnand K, Young R, et al. Dynamic contrast-enhanced texture analysis of the liver: initial assessment in colorectal cancer. Invest Radiol 2011;46:160-8.
59. Davnall F, Yip CS, Ljungqvist G, et al. Assessment of tumor heterogeneity: an emerging imaging tool for clinical practice? Insights Imaging 2012;3:573-89.
60. Chicklore S, Goh V, Siddique M, et al. Quantifying tumour heterogeneity in 18F-FDG PET/CT imaging by texture analysis. Eur J Nucl Med Mol Imaging 2013;40:133-40.
61. Yao J, Dwyer A, Summers RM, et al. Computer-aided diagnosis of pulmonary infections using texture analysis and support vector machine classification. Acad Radiol 2011;18:306-14.
62. Yoon RG, Seo JB, Kim N, et al. Quantitative assessment of change in regional disease patterns on serial HRCT of fibrotic interstitial pneumonia with texture-based automated quantification system. Eur Radiol 2013;23:692-701.
63. Korfiatis PD, Karahaliou AN, Kazantzi AD, et al. Texture-based identification and characterization of interstitial pneumonia patterns in lung multidetector CT. IEEE Trans Inf Technol Biomed 2010;14:675-80.
64. Ravanelli M, Farina D, Morassi M, et al. Texture analysis of advanced non-small cell lung cancer (NSCLC) on contrast-enhanced computed tomography: prediction of the response to the first-line chemotherapy. Eur Radiol 2013;23:3450-5.
65. Louie AV, Rodrigues G, Olsthoorn J, et al. Inter-observer and intra-observer reliability for lung cancer target volume delineation in the 4D-CT era. Radiother Oncol 2010;95:166-71.
66. Poon M, Hamarneh G, Abugharbieh R. Efficient interactive 3D Livewire segmentation of complex objects with arbitrary topology. Comput Med Imaging Graph 2008;32:639-50.
67. Bharati MH, Liu JJ, MacGregor JF. Image texture analysis: methods and comparisons. Chemometr Intell Lab Syst 2004;72:57-71.
68. Conners RW, Trivedi MM, Harlow CA. Segmentation of a high-resolution urban scene using texture operators. Comput Vision Graph 1984;25:273-310.
69. Haralick RM. Statistical and Structural Approaches to Texture. Proc IEEE 1979;67:786-804.
70. Haralick RM, Shanmugam K, Dinstein I. Textural Features for Image Classification. IEEE T Syst Man Cyb 1973;SMC-3:610-21.
71. Diot Q, Kavanagh B, Schefter T, et al. Regional normal lung tissue density changes in patients treated with stereotactic body radiation therapy for lung tumors. Int J Radiat Oncol Biol Phys 2012;84:1024-30.
72. Vinogradskiy Y, Diot Q, Kavanagh B, et al. Spatial and dose-response analysis of fibrotic lung changes after stereotactic body radiation therapy. Med Phys 2013;40:081712.
73. Mattonen SA, Palma DA, Haasbeek CJ, et al. Distinguishing radiation fibrosis from tumour recurrence after stereotactic ablative radiotherapy (SABR) for lung cancer: a quantitative analysis of CT density changes. Acta Oncol 2013;52:910-8.
74. Mattonen SA, Palma DA, Haasbeek CJ, et al. CT image feature analysis in distinguishing radiation fibrosis from tumour recurrence after stereotactic ablative radiotherapy (SABR) for lung cancer: a preliminary study. SPIE Medical Imaging 2013: Biomedical Applications in Molecular, Structural, and Functional Imaging Proceedings 2013;8672.
75. Mattonen SA, Palma DA, Haasbeek CJA, et al. editors. Assessment of response after stereotactic ablative radiotherapy (SABR) for lung cancer: can advanced CT image feature analysis predict recurrence? Canadian Cancer Research Conference; 2013; Toronto, Canada.
76. Vu CC, Matthews R, Kim B, et al. Prognostic value of metabolic tumor volume and total lesion glycolysis from 18F-FDG PET/CT in patients undergoing stereotactic body radiation therapy for stage I non-small-cell lung cancer. Nucl Med Commun 2013;34:959-63.
77. Grosu AL, Souvatzoglou M, Röper B, et al. Hypoxia imaging with FAZA-PET and theoretical considerations with regard to dose painting for individualization of radiotherapy in patients with head and neck cancer. Int J Radiat Oncol Biol Phys 2007;69:541-51.
78. Hendrickson K, Phillips M, Smith W, et al. Hypoxia imaging with [F-18] FMISO-PET in head and neck cancer: potential for guiding intensity modulated radiation therapy in overcoming hypoxia-induced treatment resistance. Radiother Oncol 2011;101:369-75.
79. Cao Y. The promise of dynamic contrast-enhanced imaging in radiation therapy. Semin Radiat Oncol 2011;21:147-56.
80. Cao Y, Pan C, Balter JM, et al. Liver function after irradiation based on computed tomographic portal vein perfusion imaging. Int J Radiat Oncol Biol Phys 2008;70:154-60.
81. Nakajima N, Sugawara Y, Kataoka M, et al. Differentiation of tumor recurrence from radiation-induced pulmonary fibrosis after stereotactic ablative radiotherapy for lung cancer: characterization of 18F-FDG PET/CT findings. Ann Nucl Med 2013;27:261-70.

Cite this article as: Mattonen SA, Huang K, Ward AD, Senan S, Palma DA. New techniques for assessing response after hypofractionated radiotherapy for lung cancer. J Thorac Dis 2014;6(4):375-386. doi: 10.3978/j.issn.2072-1439.2013.11.09